

EXPERIMENTAL AND NUMERICAL STUDIES OF WEAKLY ELASTIC VISCOUS FLUIDS IN A HELE-SHAW GEOMETRY

Diana BROBOANĂ, Tiberiu MUNTEAN, Corneliu BĂLAN

REOROM Laboratory, Hydraulics Department, "Politehnica" University of Bucharest, Romania
Corresponding author: Diana BROBOANA, 313 Splaiul Independentei, sector 6, Bucharest, Romania, fax (021)4029865,
diana@hydrop.pub.ro

The paper is focused to the experimental investigations of weakly elastic viscous flows in complex geometries, with application in biofluid mechanics. The test samples, polyacrylamide solutions in water characterized by very low relaxation times ($\lambda < 0.01$ s), have similar shear rheology with blood at medium and high shear rates. The flow configuration is a special designed "T" branch Hele – Shaw geometry, characterized by relevant separation areas. The influence of polymer concentration and Reynolds number (Re) on the vortical structures are investigated. Experiments and numerical simulations of the Newtonian and shear thinning viscous fluid are performed at $Re < 1000$. The analyses of vortices evidence the increasing of their magnitude with polymer concentration and qualitative changes in the vorticity distribution within the separation areas of weakly elastic flows, in comparison to pure Newtonian ones. The present numerical results are qualitatively similar to experiments, up to a Reynolds critical number $Re_{cr} \cong 650$. The generalized Newtonian models, which fit the shear thinning behaviour of the samples, are not able to reproduce also quantitatively the experimental evidences, so elasticity (even if is present in a very small amount) plays a relevant role in defining the flow structure within separation areas.

Key words: viscoelasticity; polymer solutions; weakly elasticity; flow visualization; biofluids; Reynolds number.

1. INTRODUCTION

A main research topic in the field of non-Newtonian fluid mechanics is focused in establishing a test procedure to validate constitutive relations for viscoelastic liquids in complex flows. The samples under investigation are in general well defined polymer solutions from the rheological point of view (as Boger, M1, S1, A1 viscoelastic liquids); their material constants are usually determined from classical viscometric tests and in some cases also from elongational experiments. The standard test flow geometries are either planar or axial-symmetric contractions or expansions ([5], [12], [16], [18], [18], [24]). Using different visualization methods or birefringence and NMR based techniques, the velocity and stress distributions in the flow field are determined experimentally. Then, following different numerical schemes and rheological models, the combined equation of motion and constitutive relation are solved for the same configurations (usually, the motion is considered isochoric) and the results of the simulations are compared with experimental patterns of velocity distributions (or pathlines) and stresses, at the same Weissenberg or Deborah numbers.

The majority of the papers is focused to concentrated polymer solution characterized by medium relaxation times, i.e. $\lambda > 0.5$ s and high value of zero shear viscosity, i.e. $\eta_0 > 1$ Pas. Limitations of the numerical procedures at high Weissenberg numbers is analyzed, but in most papers the influence of Reynolds number is not an issue of discussion, since it is aprioric considered much less than one, [12], [21].

Few papers are dedicated to the study of weakly or dilute polymer solutions in complex flow, [1], [2], [7]. For these type of samples the concentration and/or molecular mass of the polymer is small and the Reynolds number influence can not be neglected any more, especially if the solvent is water and the flow takes place in complex geometries, see also [17].

The present study is dedicated to the experimental investigation of weakly elastic polymer solution based on water and polyacrylamide, with a rheology similar to blood, [19]. The aim of the work is to compare the real spectrum of complex weakly viscoelastic flows in a Hele – Shaw branching geometry, with the corresponding numerical solutions of the shear thinning fluids, in order to detect indirectly the influence of elasticity on the flow field. We intend to apply the results to biofluid mechanics, respectively to calibrate the numerical procedure for blood flow simulations in branching large arteries. It is also of interest to detect experimentally the influence of elasticity in a complex flow of low viscous fluid, especially in the areas where flow separation is remarkable and wall shear stress reaches its minimum, see [3] and [4].

Previous works of our group ([1], [2]) put in evidence some important features related to this topic:

1. In weakly elastic polymer solution the polymer concentration is below the critical overlap concentration [9], respectively the solvent contains mainly discrete macromolecules [9]. As consequence, elasticity is not relevant in simple viscometric motions and difficult to be measured in pure extensional flows; respectively, the elastic modulus G' and the first normal difference N_1 are not measurable with commercial rheometers. We expect that only complex flows at medium and high Reynolds numbers emphasize the presence of elasticity, [22].
2. In the case of weakly elastic polymer solution with high viscosity solvent the streamline pattern in planar symmetric geometries of the pure viscous fluid at a characteristic Reynolds number $Re_i^0 < Re_{cr}$ is very similar to the streamline pattern of the viscoelastic fluid with small elasticity at a higher Reynolds number Re , $Re_i^0 < Re < Re_{cr}$ (here Re_{cr} is the Reynolds number which defines the first qualitative change of the flow regime). This means that the presence of a small amount of polymer in a very viscous liquid directly influences the onset and development of flow separation and secondary flows, in the sense that elasticity has a stabilising effect on the inertial instability (same result was obtained in [18]). The Giesekus differential constitutive relation is able to model properly this rheological behaviour for planar motions, see [1].
3. The experiments of weakly elastic polymer solution based on water in 3D branching flows at $100 < Re < 3000$ reveal the influence of elasticity on the onset of transitory flow regime, respectively the laminar motion is extended for low concentrated polymer solutions at higher Reynolds numbers, than in the case of pure viscous solvent. The experiments corroborated with numerical simulations indicate that modification due to elasticity of the extensional properties of the solution is responsible for this phenomena, see [2].
4. Practical applications of weakly elastic polymer solutions are mainly connected with the phenomena of drag reduction, where a very small amount of polymer is added to a viscous fluid in order to decrease friction in turbulent flows, [13], [14], [15]. This issue is not directly related to the present work, but some of the papers reveal important aspects, also common for our topic, as the balance between inertia and elasticity within weakly or dilute elastic solutions, [6], [10].

The samples rheology and the flow geometry investigated in the paper are presented in section 2. The experiments are performed in a Hele-Shaw “T” branch configuration; it is a 3D complex flow characterized by two dominated velocity components (the velocity normal to the cell has two orders less in magnitude) and separation flow areas which are easy observable at medium Reynolds numbers. The polymer solutions used in tests have concentrations lower than in our previous experiments presented in [2], with a maximum measured zero shear viscosity of 4 mPas. The relaxation time of solutions is assumed to be of order of 0.001 s, therefore the characteristic elasticity number

$$El = \frac{Wi}{Re} = \frac{2\lambda\eta_0}{\rho h^2} \quad (1)$$

is less than 0.01 (here h is the space scale, ρ is the mass density and Wi is the Weissenberg number). At this low values of El -number, the elasticity influence is founded irrelevant, not only in simple flows, but also in symmetric complex geometries (e.g. contraction or expansions flows), [5], [20]. This is the main reason why we decided to use the “T” non-symmetric branch flow configuration. The section 3 of the paper is dedicated to the flow visualizations of vortices at different Reynolds numbers, $200 < Re < 3000$, and their evolution with increasing of polymer concentration. The numerical simulations of the corresponding flows for the

Newtonian fluid and polymer solution at maximum concentration used in experiments are presented in section 4.

The paper provides new experimental results of weakly elastic flows in a complex geometry with relevant vortices areas, which might be used to interpret more realistic the blood simulations in branching flows. The conclusions of the work are consistent with the previous papers published by the authors and point some important experimental aspects which distinguish viscoelastic flows with low elasticity from the pure viscous ones.

2. EXPERIMENTAL AND SAMPLES RHEOLOGY

2.1 Rheology of polymer solutions

In this study, elastic properties of the test liquids have been obtained by adding to a Newtonian solvent (water with density $\rho_s = 1000 \text{ kg/m}^3$ and viscosity 1.05 mPas) pieces of concentrate solution of polyacrylamide with density $\rho_p = 1020 \text{ kg/m}^3$ (molecular weight $M_w = 2 \cdot 10^5 \text{ g/mol}$) dissolved in water, in different mass concentrations from C_{01} to C_5 . The polymer solution with concentration C_i is obtained by mixing for one day the previous sample of concentration C_{i-1} with additional 2 grams of concentrate solution (the total mass of water used in experiments is 4 kg). Each test solution is identified by its shear viscosity function measured immediately at the end of experiments (a probe of 20 g was also collected for oscillatory rheological tests). The shear experiments were performed with Physica MC 1 (double gap concentric cylinders) and Physica MC 300 (cone – plate geometry) was used for the oscillatory test.

The variations of the dynamic moduli (i.e. elastic modulus G' and loss modulus G'') as a function of concentration and frequency are shown in Fig. 1, for the initial concentrate polyacrylamide solution (CPS) and concentration C_5 , respectively in Fig. 2 for concentrations C_1 to C_5 . Below the threshold concentration $C^* < C_1$ the elastic modulus is not measurable (here C^* might be considered the upper limit for the dilute polymer solution, see also [9], [11]). The test solutions at concentrations $C_{0i} < C^*$ ($i = 1, 4$) are defined as weakly elastic, hence they are characterised by relaxation times less than 0.01 s , [5]. In Fig. 3 are represented the corresponding shear viscosity of the weakly elastic samples used in the present study. The rheological tests, as well as the visualization experiments, have been performed at temperature of 22° C .

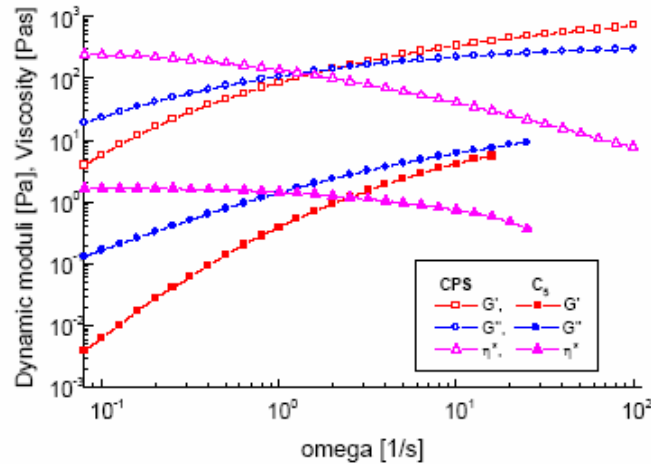


Fig. 1. Rheological properties of the concentrate polymer solution (CPS) and concentration C_5 in dynamic test.

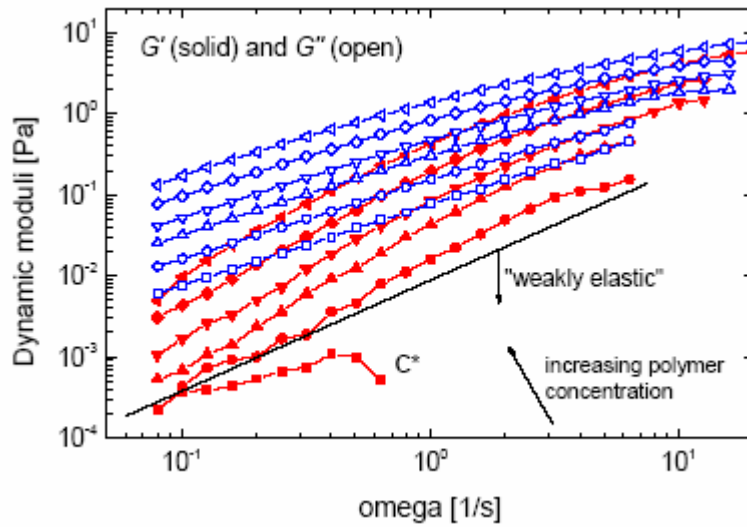


Fig. 2. Rheological properties of the polymer solutions at concentrations $C_1 - C_5$; below concentration C_1 the solution is considered weakly elastic, see also [2].

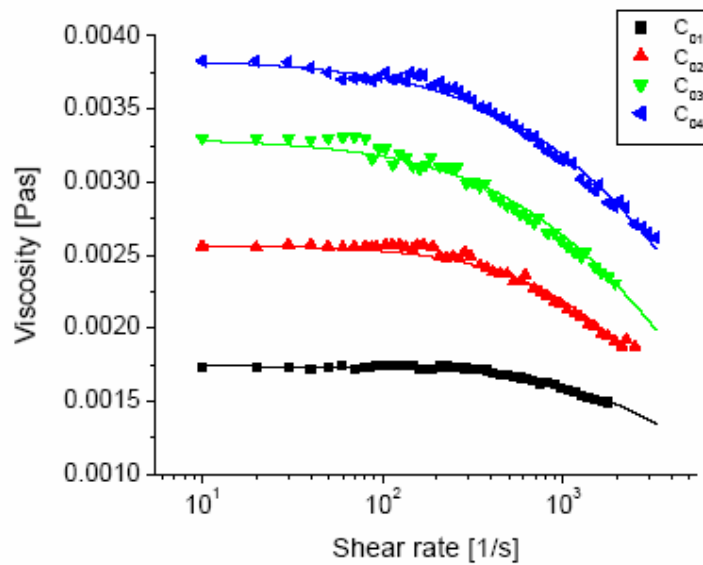


Fig. 3. Shear viscosity of the tested samples; the polymer concentrations $C_{01}-C_{04}$ are below concentration C^* from Fig. 2; the fitting of experimental data is made with relation (3).

2.2 Experimental set-up

The experiments have been performed in the REOROM Laboratory from U. P. Bucharest. The test device is basically a Hele-Shaw cell: the fluid flows in a symmetric “T” branch profile between 2 transparent horizontal parallel planes with a gap of $\delta = 2$ mm, see Fig. 4. The abrupt change in direction of the stream generates two main vortices, see detail A from Fig. 4 (here the length L defines the magnitude of vortex I). The flow separation areas are well evidenced at $Re > 200$ and the evolution of vortices I and II (respectively the characteristic ratio L/B and the internal velocity field) are observed as function of Re magnitude.

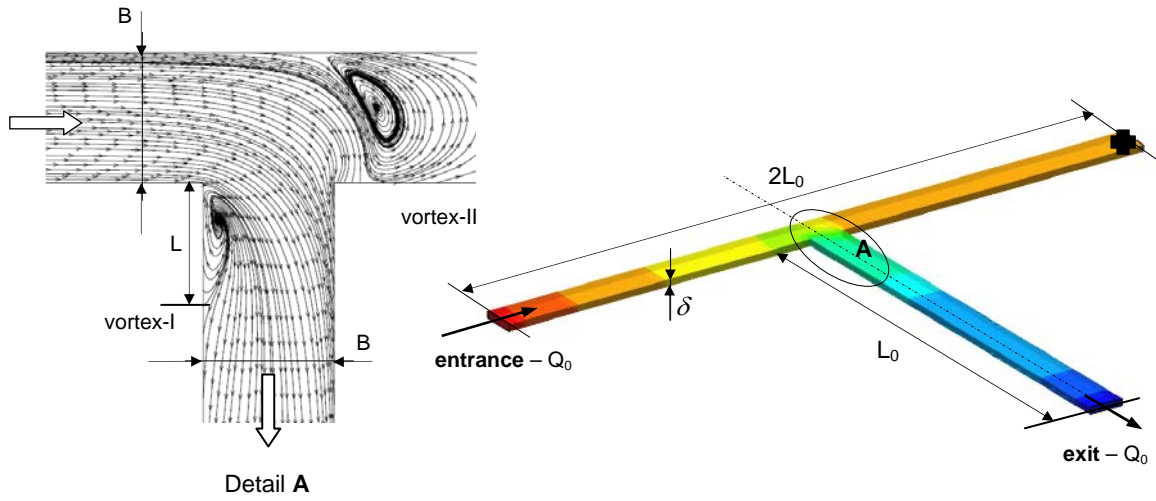


Fig. 4. Flow test geometry: Hele-Shaw “T” profile with $L_0 = 250$ mm, $B = 25$ mm and gap $\delta = 2$ mm; detail A shows the stream trace configuration on the middle plan in vicinity of the junction and the location of the vortices I and II (numerical simulation at $Re = 700$).

The experimental space scale is $4R_h$, where $R_h \cong \delta/2$ is the hydraulic radius. The characteristic Reynolds number is computed with the formula

$$Re = \frac{\rho V_m 2\delta}{\eta_0} \quad (2)$$

where $V_m = Q_0/(\delta B)$ is the mean velocity at the entrance, Q_0 is the flow rate and η_0 is the zero shear viscosity. The modified Cross model, i.e.

$$\eta := \eta_s + \frac{\eta^*}{1 + (k \dot{\gamma})^{1-n}} \quad (3)$$

was used for numerical fitting of the viscosity function. In (3) $\eta_s = 1$ mPas is the water viscosity; η^* , k and n are the corresponding constants of the Cross model, with $\eta_0 := \eta_s + \eta^*$.

Tab. 1. Values of the material parameters for the tested samples; the model (3) was using for fitting the experimental data from Fig. 3.

Material parameters	Concentration C_{01}	Concentration C_{02}	Concentration C_{03}	Concentration C_{04}
η^* [Pas]	0.0007	0.0016	0.0023	0.0028
k [s]	0.00009	0.00018	0.0002	0.00018
n [-]	0.0001	0.00137	0.1936	0.21

The fluid is re-circulated in the installation by a special volumetric pump which provides a constant flow rate within the interval $Q_0 \in [0.5, 7.5]$ l/min. The procedure to visualize the steady flow field is based on the classical streak line photography procedure, see [2] and [8]: small particles are introduced in the flow area and their path lines are recorded with a high resolution Digital Camera (DC-Minolta Dimage 7 at 5.5 Megapixels; the expose time and lens aperture are dependent on the velocity magnitude and the intensity of light). As reflecting particles are used very small hydrogen bubbles (mean diameter of 20 microns) generated in the flow stream at the inlet of the tested geometry by electrolyze procedure. The experimental investigation is focused to the visualization of vortex-I and the determination of its magnitude and characteristics, as function of polymer concentration and the magnitude of Reynolds number.

3. FLOW VISUALIZATION

Visualizations of vortex-I have been performed for concentrations C_0 to C_{04} in the interval $Re \in (200-3000)$. For each concentration have been obtained at least 15 pictures of the streak lines distribution at different Reynolds numbers. The main geometric parameter which defines the magnitude of vortex I is the length L , i.e. the distance from the junction to the re-attachment point of the main current, down stream the flow separation, see Fig. 4 – detail A. In experiments, the exact location of the point which limits the separation area (vortex I) is difficult to be observed, especially at high Reynolds numbers. So, we take L as the distance from the junction to the line where the mean velocity vectors from the bulk of the flow are parallel to the wall, see Fig. 5. Some pictures of the vortex-I for water (i.e. concentration C_0) are shown in Fig. 5 (here we show also a visualization at $Re = 9300$). In Fig. 6 is presented the evolution of vortex-I with concentration and Reynolds number, at constant flow rate ($V_m = 0.66$ m/s). The Figure 7 discloses the structure and magnitude of vortex-I for concentration C_{04} and in Fig. 8 are shown, for comparison, the path lines distributions for concentrations C_0 , respectively C_{02} , at two values of the Reynolds number.

The analyse of visualizations of vortex-I evidences two main conclusions:

1. At the same concentration, the length L is increasing with increasing Reynolds number, see Fig. 5 for C_0 and Fig. 7 for C_{04} . It is also evident that a transition from laminar to turbulent motion is observed for water in the range $Re \in (1000, 1600)$, see Fig. 5.
2. The length L seem to be independent on polymer concentration for the tested samples, if the flow rate is maintained constant and $Re > 600$. At the same Reynolds number and $Re < 1000$, the vortex I becomes larger with increasing concentration, but with diminished intensity of inside circulation, see in Fig. 6 the qualitative differences between the vortex I for concentrations C_{01} ($Re = 1530$) and C_{02} ($Re = 1000$) and also Fig. 8.

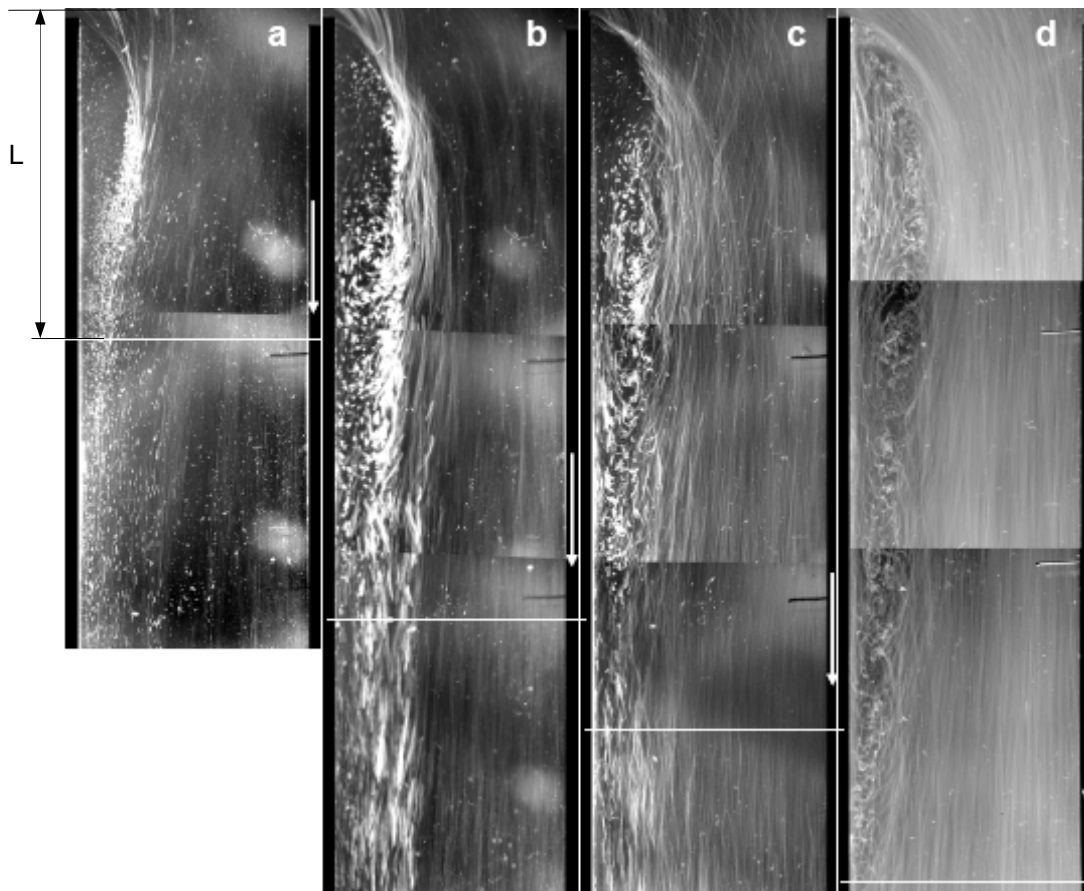


Fig. 5. Evolution of vortex-I for water with increasing Reynolds number:
a) $Re = 1000$, b) $Re = 1600$, c) $Re = 2600$, d) $Re = 9300$.

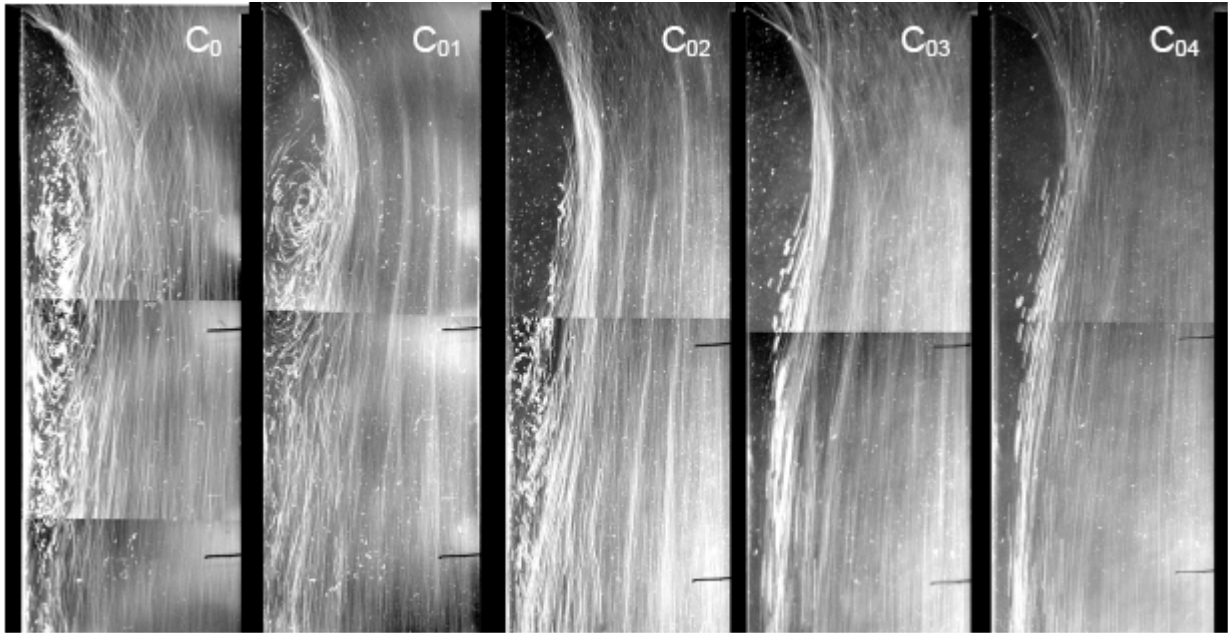


Fig. 6. Evolution of vortex-I with concentration, at constant velocity ($V_m = 0.66$ m/s): $C_0 - Re = 2600$, $C_{01} - Re = 1530$, $C_{02} - Re = 1000$, $C_{03} - Re = 790$, $C_{04} - Re = 685$.

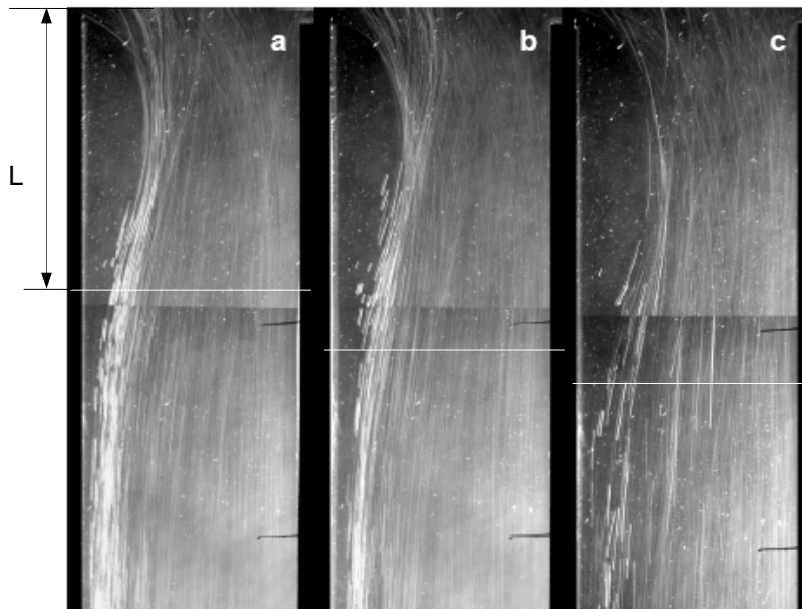


Fig. 7. Evolution of vortex-I with Re -number at concentration C_{04} :
a) $Re = 520$, b) $Re = 685$, c) $Re = 850$.

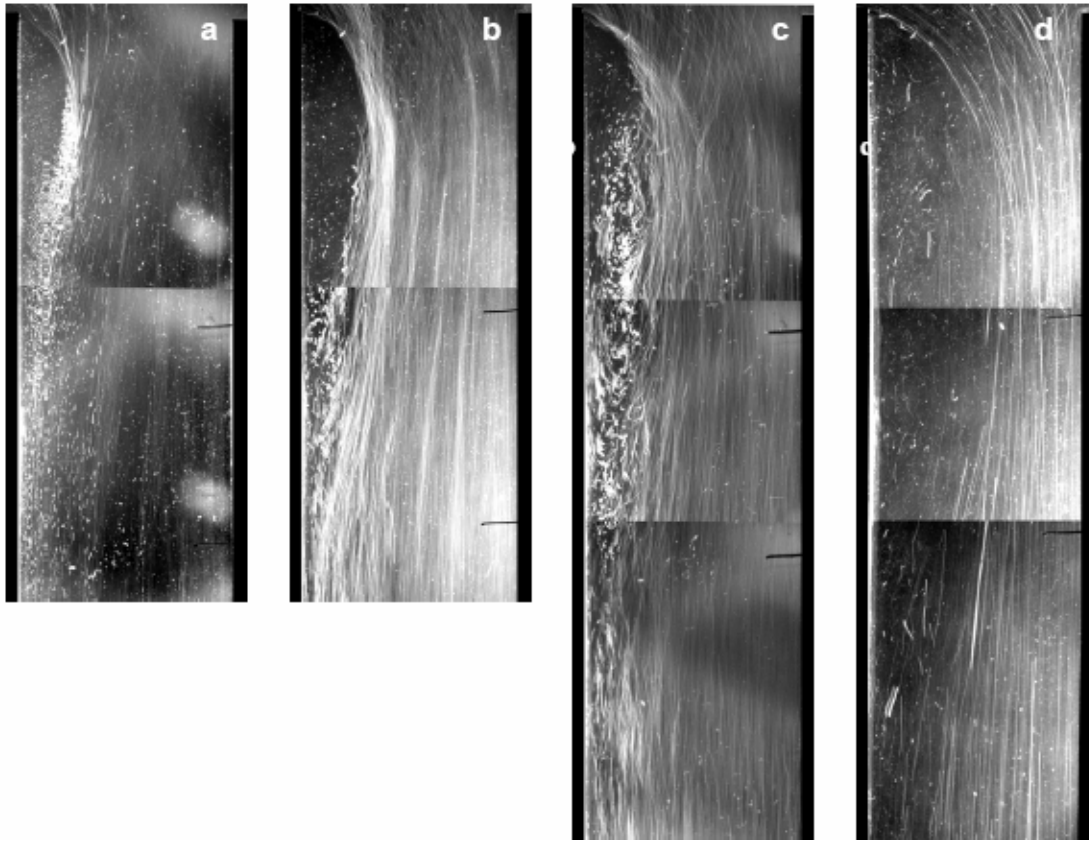


Fig. 8. Structure of vortex-I for water: a) $Re = 1000$ ($V_m = 0.24$ m/s), c) $Re = 2600$ ($V_m = 0.66$ m/s) and for concentration C_{02} : b) $Re \cong 1000$ ($V_m = 0.48$ m/s), d) $Re \cong 2600$ ($V_m = 1.1$ m/s). At the same Reynolds number the vortex corresponding to a higher concentration is larger.

From the comparison of Fig. 8.c with Fig. 8.d. one can notice that the presence of polymer delay the onset of turbulent motion: at $Re = 2600$ and concentration C_{02} the motion discloses still laminar characteristics (Fig. 8.d), in comparison to the flow of water (Fig. 8. c) where turbulence patterns are present. These experimental evidences are consistent with the previous results of the authors, [2], i.e. the onset of turbulent regime in a similar Hele-Shaw geometry was “shifted” by the presence of polymer at higher Reynolds numbers, than in the case of the pure Newtonian flows (see also the observations and conclusions published in [18]).

The present experimental investigations have some limits, especially at small velocities where the visualization procedure is not able to produce quality pictures. Also, due to elasticity of the samples, the air bubble used as tracers for visualizations penetrate with difficulty inside the vortex at low current velocity. Therefore, the internal vortex motion is not well evidenced in our experiments. The analyse of the data as function of Reynolds number are more qualitative and less quantitative. The definition of the Reynolds parameter for shear thinning fluids is not well established, since the viscosity varies with the strain rate in the flow field and the local kinematics is unknown. Each constitutive model determine another formula for the Reynolds number; for that reason we have decided to use the formula (2) for all tested samples, even though it is not exact for the shear thinning fluids.

5. NUMERICAL SIMULATIONS

In the arterial branching flows, the most important parameters are the wall shear stress magnitude and the location of stagnation (re-attachment) point, where the wall shear stress is zero. It is now well known that stenosis are present in the areas of vortices and the cell adhesion at the wall of arteries are starting from

stagnation points, see [3], [4] and [23]. Some numerical results of the wall shear stresses distribution in “T” branches pipes and the corresponding vorticity distributions are presented in [4].

Evident, the wall shear stress is directly related to the vortices intensity, respectively to the wall velocity gradient. The present experimental investigations put in evidence possibilities to influence the vortex and the wall shear stress configuration by adding small amount of elasticity to the viscous liquid.

Since the direct measurements of wall shear stresses are difficult, one can assume that computational results are good enough if the numerical path lines distribution is very close to the experimental visualizations.

The first sets of numerical simulations have been performed with 2D-planar and 3D “T” branch geometries using the pure Newtonian fluid and the Cross model C_{04} (corresponding to polymer concentration C_{04} , see Tab. 1), using the commercial FLUENT 6.0 code. All simulations have been performed for constant inlet velocity using the laminar unsteady segregate solver, with the time step of 0.001 s and precision of 10^{-5} . The results are displayed after 2 seconds from the onset of motion, where the asymptotic steady state is achieved for all investigated cases.

The 2D-planar simulations are qualitatively consistent with experiments, but dimension L associated to vortex-I is much extended than in reality, see Fig. 9 and Fig. 7 for comparison with experiments (at $Re > 500$ stable numerical solutions are difficult to be obtained; we have to remark that in 2D cases the characteristic length for Reynolds computation is the channel width B).

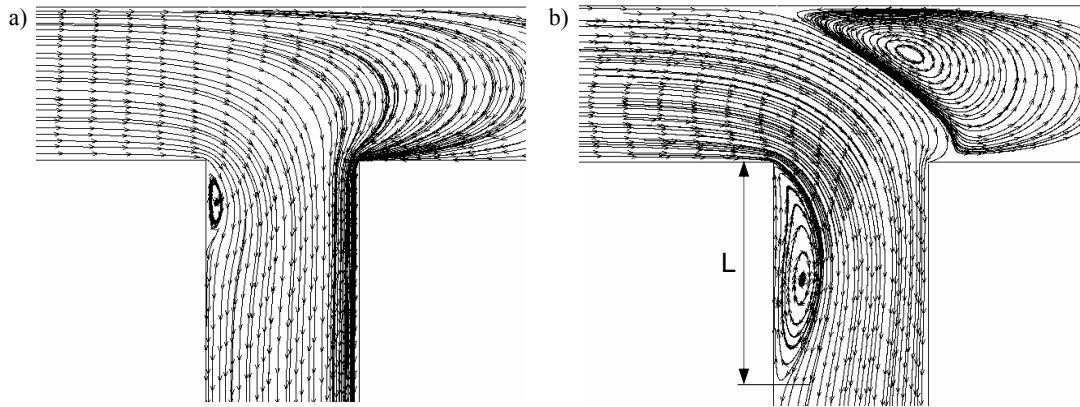


Fig. 9. Numerical simulation of the 2D “T” branch flows of the Cross model C_{04} at $Re = 125$ (a) and $Re = 250$ (b).

In Fig. 10, the 3D Hele-Shaw flow patterns of vortices I and II are represented in the middle plane of the geometry, in the range $Re \in (200, 900)$. In Fig. 11 the 3D flow structure is displayed at $Re = 550$. Here the normal section A-A is located downstream the vortex, at the distance $y = 30$ mm from the junction, see also Fig. 10.b.

Same simulations have been performed with the Newtonian model, where the zero shear viscosity is constant for all strain rates. In Newtonian computations the velocity has been maintained at the same value as for the shear thinning simulations. The comparison between the two models and the experiments for concentration C_{04} are presented in Fig. 12, where the dependence $L/B(Re)$ is shown. In Fig. 12 are also plotted the experimental points obtained for concentration C_{04} (see also Fig. 7).

One can observe that both fluid models disclose same features, consistent from qualitative point of view with experiments: (i) increasing of the vortex dimension with Reynolds number, (ii) evidence the presence of a critical value for Reynolds number, beyond which the flow regime is changed (i.e. the laminar solver does not produce realistic solutions for $Re > Re_{cr}$).

The Cross model simulations fits quite well also quantitatively the experiments for $Re < Re_{cr} \cong 670$. Therefore, the shear thinning fluids can be used successfully, as a first approximation, to represent the real complex flows of weakly elastic polymer solutions at small and moderate Reynolds numbers.

Of course, more accurate numerical solutions have to include also elasticity (which is responsible for the difference observed in Fig. 12 between the Cross solution and experiments). Different viscoelastic

models are implemented in the POLYFLOW code, but at this moment the REOROM group can not access this program.

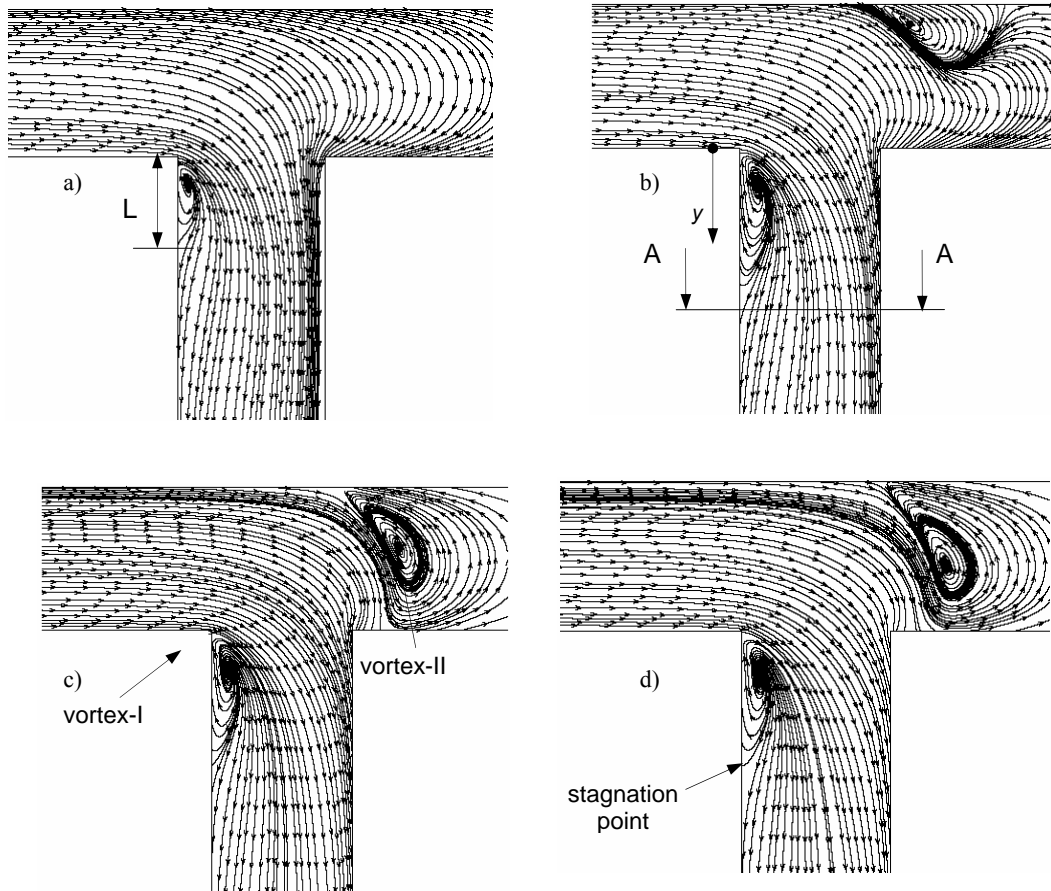


Fig. 10. Numerical simulation of the 3D “T” branch flows of the Cross model C_{04} at $Re = 220$ (a), $Re = 550$ (b), $Re = 700$ (c) and $Re = 830$ (d).

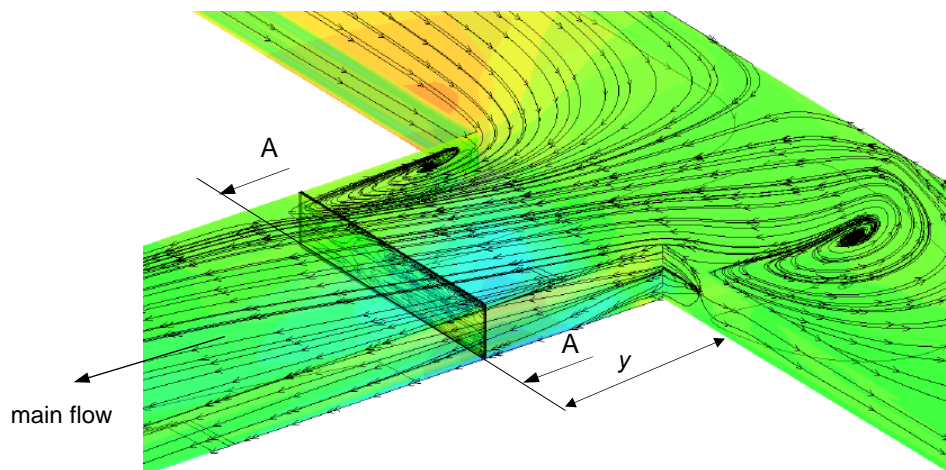


Fig. 11. 3D flow spectrum in vicinity of the junction (Cross model C_{04} , $Re = 550$).

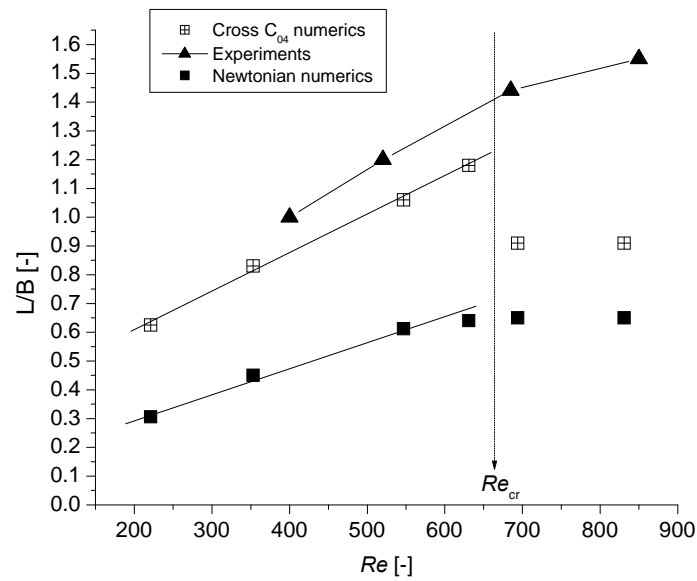


Fig. 12. Dependence $L/B(Re)$ for numerical simulations and experiments.

Once the numerical solution is validated by experiments, one can investigate the flow field in more details and extract value information for the cases of interest. For example, the vorticity magnitude and the wall shear stresses are computed, for the Newtonian and Cross C_{04} models, in vicinity of the vortex-I, see Fig. 13. Here, the component of wall shear stress along the wall (WSS_y) reaches zero magnitude in the very vicinity of the stagnation point (see Fig. 10.d), simultaneous with the minimum value for the vorticity. Important remark from this result is the following: inside the flow separation area, the Newtonian vorticity magnitude is smaller than the shear thinning one, contrary to the region outside the vortex-I (same with the absolute value of the wall shear stress).

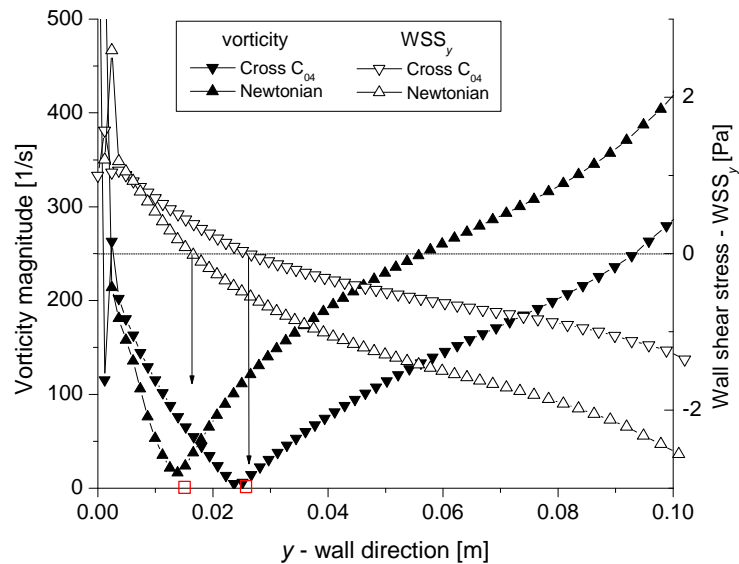


Fig. 13. Distribution of vorticity magnitude and wall shear stress in the region of vortex I; the approximative location of separation points are marked.

In Fig. 14 and Fig. 15 are presented, for comparison between the Newtonian and Cross solutions, the vorticity and stream traces corresponding to the vortex I. All results are consistent with the experimental

evidence that shear thinning character of the fluid increases the vortex-I (and also change the flow structure within the separation areas, see Fig. 14).

Another problem of interest for biofluids applications is the investigation of secondary flows, i.e. the motion which take place in normal planes to the main flow direction (the structure of secondary flows is responsible for the spin of cells and their membrane configuration). In Fig. 16 is shown the evolution of secondary flows with Reynolds number, immediately beyond the vortex-I, see Fig. 11. The Dean flow structure (i.e. the pairs of secondary vortices) are remarkable even in a Hele-Shaw geometry, but at relatively high Reynolds numbers, see Fig. 12.c-d. The simulations also evidence the existence of a “saddle like point” in the normal planes to the main flow. That points, which diverge the secondary flows, are closer to the vortex-I with increasing the Reynolds number.

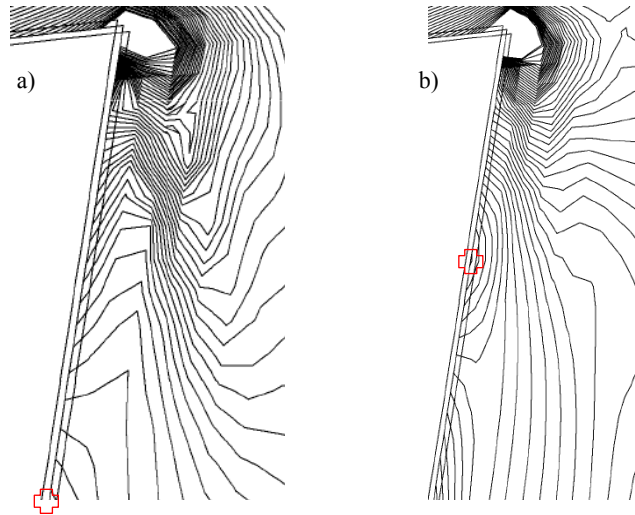


Fig. 14. Vorticity distribution on the middle plane, in the region of vortex I, for the Cross model C_{04} (a) and the Newtonian fluid (b), at $Re = 550$ (minimum vorticity points are marked).

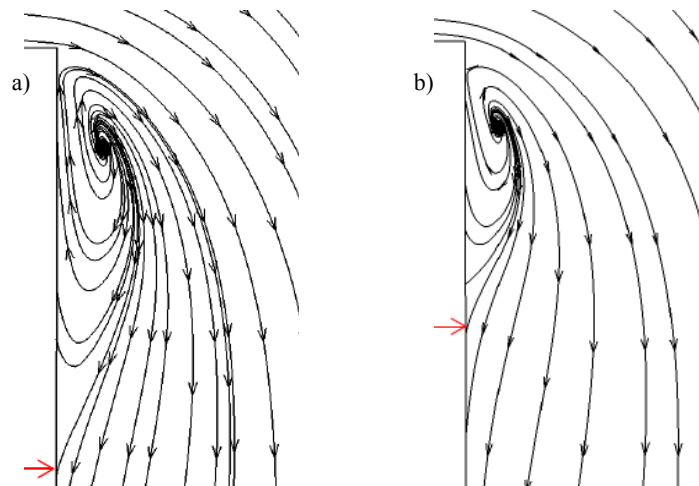


Fig. 15. Streamlines distribution on the middle plane, in the region of vortex I, for the Cross model C_{04} (a) and the Newtonian fluid, at $Re = 550$ (the separation point is marked).

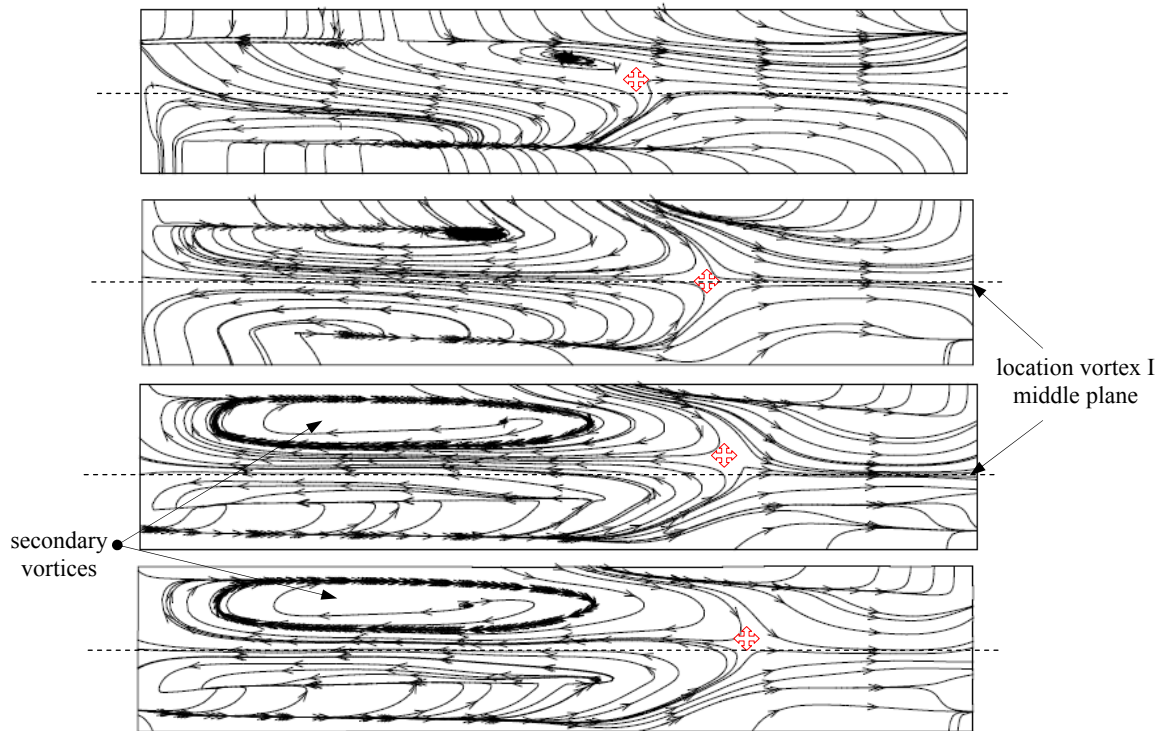


Fig. 16. Secondary flows in section A-A ($y = 30$ mm) for the Cross model C_{04} at different Reynolds numbers: $Re = 220$ (a), $Re = 550$ (b), $Re = 630$ (c) and $Re = 700$ (d); the “saddle points” are marked (here the main flow is perpendicular to the plane of represented figures).

In Fig. 17 and Fig. 18 secondary flows are evidenced more close to the vortex-I region, at the distance $y = 20$ mm from the junction. At $Re = 220$ we are still beyond the vortex I for both models, see Fig. 17. The flow structures are similar for the Newtonian and Cross fluids, also the location of the “saddle point”.

At higher Reynolds number, $Re = 630$, the pictures relieve major differences for the secondary flows inside the vortex-I, see fig. 18. At this stage of investigation, one can assume that not only the magnitude of vortex-I make the difference between a Newtonian and a shear thinning fluid, but also the 3D flow structure inside the Hele-Shaw geometry.

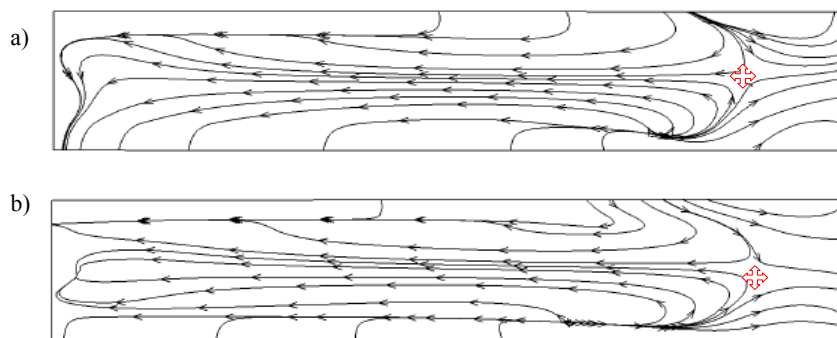


Fig. 17. Secondary flows at $Re = 220$, in section A-A at $y = 20$ mm, for the Cross model C_{04} (a) and the Newtonian fluid (b).

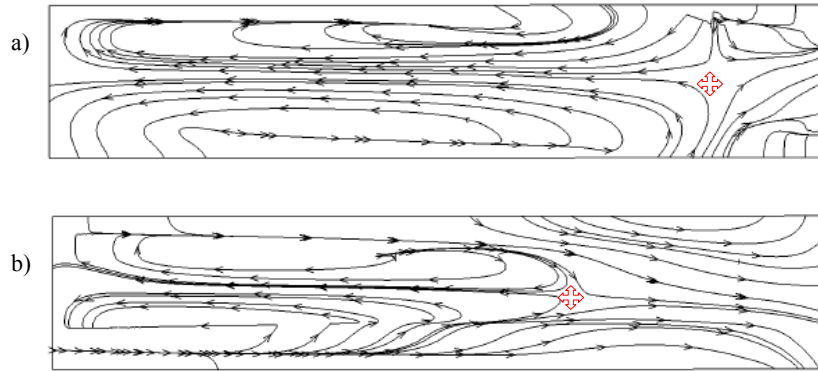


Fig. 18. Secondary flows at $Re = 630$, in section A-A at $y = 20$ mm, for the Cross model C_{04} (a) and the Newtonian fluid (b).

The present numerical simulations disclose relevant information on the flow field and fluid structures in the area of vortices. In particular, the evolution and magnitude of wall shear stresses are computed. For biofluid applications the results are valuable and offer a better framework in understanding the blood flows in branching geometries.

5. FINAL REMARKS

The work presented experimental investigations and numerical simulations of pure viscous and weakly elastic viscous flows in a branching Hele-Shaw geometry. The study is focused on the behaviour of a polymer solution based on water and polyacrylamide in the area of flow separation, up to a Reynolds number of 1000. The weakly elastic samples are modelled with the Cross shear thinning fluid and the computations were performed with the FLUENT code 6.0.

The experimental analyses of vortices evidence that, at constant Reynolds number, their magnitude is increasing with polymer concentration. Same results are obtained for the numerical simulations, respectively the shear thinning character increase the magnitude of the vortices and move the separation point down stream, in comparison to the linear Newtonian case. The analyses of vortices also evidence the increasing of their magnitude with polymer concentration and qualitative changes in the vorticity distribution within the separation areas.

The numerical results are only qualitatively consistent with experiments, since the experiments disclose larger vortices than computations. The Cross model is not able to reproduce properly all the experimental features (i.e. as flow field inside separation areas), despite the fact that it fits the shear thinning behaviour of the samples obtained for the rheological tests. This evidence is due to the absence of elasticity in the generalized Newtonian constitutive relations. Even in small amount, the presence of elasticity produce significant effects on the flow field, if relevant extension of the fluid is present, and this is the case of the 3D branches flows which generate remarkable vortices.

The flow visualizations of weakly elastic viscous fluids in complex geometries at small and moderate Reynolds numbers have an intrinsic value, since the experimental results can be used for testing the performing of different constitutive relations in modeling viscous and viscoelastic flows.

The aim of the paper was to model the flow of a similar fluid with blood in a branching geometry, at the values of Reynolds number which are met in real flows in arteries. The final goal of our work is to establish a numerical procedure able to deliver valuable information for the characterization of real flows in branching arteries, especially in relation to the developing of stenosis, recirculation areas and flow separations. One main hemodynamic parameter of interest is the value of wall shear stresses, which can be obtained only by numerical computations.

Further investigations are needed, especially in relation to the capture of elasticity influence on the development of vortical structures within the branches. This is the target of the research of REOROM group in the near future.

ACKNOWLEDGEMENTS

The authors acknowledge the financial support received from CNCSIS grants no. 16/2004 and 1368/2006 and CEEEX project CARDIOCOMP/2006.

REFERENCES

1. BALAN C., LEGAT V., NEAGOE A., NISTORAN D., Experimental investigations and numerical simulations for an open channel flow of a weakly elastic polymer solution around a T-profile, *Exp. Fluids*, 36(2004) 408-418
2. BALAN, C., BROBOANA, D., MUNTEAN, T., Experimental and numerical investigations of viscous and weakly elastic viscous flows in bifurcations, *Trends in Appl. of Math. to Mech.*, Shaker Verlag, Aachen, 2005, pp. 67-74
3. BERGER S.A., L-D. JOU L-D., Flows in stenotic vessels, *Annu. Rev. Fluid Mech.*, 32(2000) 347-382
4. BROBOANA D., MARCULESCU M., KADAR R., BALAN C., Experimental and numerical simulations of 3d branching flows, with application to the modeling of blood flow in arteries, *Timisoara Med. Journal*, 56(2006) 69-74
5. BYARS J.A., BINNINGTON R.J., BOGER D.V., Entry flow and constitutive modelling of fluid S1, *J. Non-Newtonian Fluid Mech.*, 72(1997) 219-235
6. CADOT O., Partial roll-up of a viscoelastic Kármán street, *Eur. J. Mech. B – Fluids*, 20(2001) 145-153
7. CHIBA K., NAKAMURA K., Instabilities in a circular entry flow of dilute polymer solutions, *J. Non-Newtonian Fluid Mech.*, 73(1997) 67-80
8. DEVASENATHIPATHY S., SANTIAGO J., WERELEY S.T., MEINHART C.D., TEKEHARA K., Particle imaging techniques for microfabricated fluidic systems. *Exp. Fluids*, 34(2003) 504-514
9. HARRISON G.M., REMMELGAS J., LEAL, G., The dynamics of ultradilute polymer solutions in transient flow: Comparison of dumbbell-based theory and experiments, *J. Rheol.*, 42(1998) 1039-1058
10. HOUSIADAS K.D., BERIS A.N., Polymer-induced drag reduction: effects of the variations in elasticity and inertia in turbulent viscoelastic channel flow, *Phys. Fluids*, 15(2003) 2369-2384
11. KALASHNIKOV V.N., Degradation accompanying turbulent drag reduction by polymer additives, *J. Non-Newtonian Fluid Mech.* 103(2002) 105-121
12. KIM J-H, OZTEKIN A, NETI S (2001) Non-linear dynamics of viscoelastic flows in axisymmetric conduits with abrupt changes, *J Non-Newtonian Fluid Mech.*, 97(2001) 169-193
13. KOELTZSCH K., QI Y., BRODKEY R.S., ZAKIN J.L., Drag reduction using surfactants in a rotating cylinder geometry, *Exp. Fluids*, 34(2003) 515-530
14. LARSON R.G., Analysis of polymer turbulent drag reduction in flow past a flat plate, *J. Non-Newtonian Fluid Mech.*, 111(2003) 229-250
15. MIN T., CHOI H., YOO J.Y., Maximum drag reduction in a turbulent channel flow by polymer additives, *J. Fluid Mech.*, 492(2003) 91-100
16. MOMPEAN G., THOMPSON R.L., SOUZA MENDES P.R., A general transformation procedure for differential viscoelastic models, *J. Non-Newtonian Fluid Mech.* 111(2003) 151-174
17. MCKINLEY G.H., PAKDEL P., OZTEKIN A., Rheological and geometric scaling of purely elastic flow instabilities, *J Non-Newtonian Fluid Mech.*, 67(1996) 19-47
18. OLIVEIRA P.J., Asymmetric flows of viscoelastic fluids in symmetric planar expansion geometries, *J. Non-Newtonian Fluid Mech.*, 114(2003) 33-63
19. POHL M., WENDT M.O., KOCH B., VLASTOS G.A., Mechanical degradation of polyacrylamide solutions as a model for flow induced blood damage in artificial organs, *Biorheology*, 37(2000) 313-324
20. PURNODE B., CROCHET M.J., Flows of polymer solutions through contractions part I: flows of polyacrylamide solutions through planar contractions, *J Non-Newtonian Fluid Mech* 65(1996) 269-289
21. ROTHSTEIN J.P., MCKINLEY G.H., The axisymmetric contraction-expansion: the role of extensional rheology on vortex growth dynamics and the enhanced pressure drop, *J Non-Newtonian Fluid Mech.*, 98(2001) 33-63
22. WALTERS K., WEBSTER M.F., On dominating elastico-viscous response in some complex flows, *Phil. Trans. R. Soc. Lond. A* 308(1982) 199-218
23. YAMAGUCHI R., Flow structure and variation of wall shear stress in asymmetrical arterial branch, *J. Fluids Structures*, 13(1999) 429-442
24. ZIRNSAK, M.A., BOGER, D.V., Axisymmetric entry flow of semi-dilute xanthan gum solutions: prediction and experiment, *J. Non-Newtonian Fluid Mech.*, 79(1998) 105-136

Received February 22, 2007